View Online / Journal Homepage / Table of Contents for this issue
Dynamic Article Links

Journal of Materials Chemistry

Cite this: J. Mater. Chem., 2011, 21, 9674

www.rsc.org/materials

PAPER

DNA-based fabrication of density-controlled vertically aligned ZnO nanorod arrays and their SERS applications†

Lanlan Sun, Dongxu Zhao,* Zhenzhong Zhang, Binghui Li and Dezhen Shen

Received 25th February 2011, Accepted 5th April 2011
DOI: 10.1039/c1jm10830a

We described a novel seeded synthesis of vertically aligned ZnO nanorod arrays on a DNA network surface. Zinc ions were first adsorbed onto the DNA network and then heated to yield layers of ZnO seeds. The DNA network plays an important role not only as a substrate for the adsorbing of zinc ions, but also as a fine template for density controllable synthesis of high-quality ZnO seeds. The density of ZnO seeds was controlled by the adsorption times of zinc ions. The final density of ZnO nanorods was determined mainly by that of ZnO seeds. The ZnO nanorod arrays were used as templates for making silver-coated ZnO nanocomposites, which were applied as substrates in surface-enhanced Raman scattering (SERS) measurements. Two typical probe molecules, R6G and 4-ATP were used to test the SERS activity of the ZnO/Ag composites and the results indicated good Raman activity on the substrate.

Downloaded by Changchun Institute of Optics, Fine Mechanics and Physics, CAS on 23 April 2012
Published on 17 May 2011 on http://pubs.rsc.org | doi:10.1039/C1JM10830A

1. Introduction

DNA molecules are attractive biological templates to construct nanostructures with a specific shape and unique properties. DNA is a rigid biopolymer that can withstand a range of pH, temperature, and solvation conditions. Particularly, DNA possesses a linear structure, large aspect ratio (length/diameter) and well-defined sequences of DNA base and a variety of superhelix structures. The negatively-charged phosphate groups of DNA have a strong affinity for the metal cations and positively-charged nanoparticles. In the past decades, metal nanowires (silver, gold, platinum, palladium, copper), carbon nanotube and semiconductor nanowires (ZnO, CdS, PbS and ZnS) were created using DNA as a template.[1–10] In addition to linear structure, large-scale DNA networks can also be fabricated by controlling DNA concentration.[11] Wei *et al.* have fabricated nanoporous silver films by the electrostatic self-assembly of silver nanoparticles onto DNA network.[12]

Zinc oxide (ZnO) is an n-type, wide band gap ($E_g = 3.35$ eV) semiconductor, with a large excitation binding energy of 60 meV.[13] ZnO exhibits a variety of properties, including transparent conductivity, piezoelectricity, ferromagnetic and gas sensing properties.[14–17] ZnO nanostructures can be grown on a variety of substrates including sapphire, glass, silicon, and indium-tin-oxide (ITO).[18] Recently, highly ordered ZnO nanorods or nanowires are particularly important for their potential applications in optics, optoelectronics, sensor and photocatalysts.[18–21] ZnO nanorods arrays were also used as a template to fabricate ZnO/Au composites, which showed highly enhanced surface enhanced Raman scattering activity.[22] Therefore, many different synthetic methods, including chemical vapor deposition, hydrothermal methods, template-based methods, pulsed laser deposition, metal–organic source vapor deposition and sol–gel have been introduced to prepare ZnO nanorods or nanowires.[23–28] In addition, ZnO is a biocompatible semiconductor, and it has been shown that ZnO nanorods are compatible with DNA.[29] Usually, highly vertical ZnO nanowire arrays are synthesized either with an appropriate single crystalline substrate (Al_2O_3 or GaN) or with a textured ZnO thin film as a nucleation layer that is deposited on a nonepitaxial substrate (such as silicon or glass). These methods are always limited to insulating or expensive substrates, and the ZnO thin film requires gas-phase fabrication of the ZnO layer. To overcome these limitations, Yang *et al.* developed a hydrothermal process for preparing ZnO nanowires arrays using textured ZnO seeds.[30]

Here, we expanded the seeded synthetic methods to prepare density-controllable ZnO nanorod (NR) arrays using a mild solution process. ZnO seeds were formed directly on substrates by thermally decomposing zinc acetate that adsorbed on DNA networks at 350 °C. The final density and size of the ZnO NRs were determined mainly by those of ZnO seeds. In the optimized procedure, highly-quality vertical ZnO NR arrays were grown, which were used as templates for making silver-coated ZnO (ZnO/Ag) composite nanoarrays. It was found that these ZnO/Ag composite nanoarrays could be used as good SERS-active substrates with Rhodamine 6G (R6G) and 4-aminothiophenol (4-ATP) as test probes.

Key Laboratory of Excited State Processes, Chinese Academy of Sciences, Changchun Institute of Optics, Fine Mechanics and Physics, Chinese Academy of Sciences, 16 East Nan-Hu Road, Open Economic Zone, Changchun, 130033, People's Republic of China. E-mail: dxzhao2000@yahoo.com.cn; Fax: +86-431-4627031; Tel: +86-431-86176322

† Electronic supplementary information (ESI) available. See DOI: 10.1039/c1jm10830a

This journal is © The Royal Society of Chemistry 2011

Downloaded by Changchun Institute of Optics, Fine Mechanics and Physics, CAS on 23 April 2012
Published on 17 May 2011 on http://pubs.rsc.org | doi:10.1039/C1JM10830A

2. Experimental section

2.1 Materials

Lambda DNA (λ-DNA, 0.3 mg mL^{-1}, 48502 bp) was purchased from Sino-American Biotechnology Company (Beijing, China). Zinc acetate dehydrate ($ZnAc_2 \cdot 2H_2O$) and 4-aminothiophenol (4-ATP) were purchased from Aldrich. Hexamethylene tetramine (HMT) and Rhodamine 6G (R6G) were purchased from Exciton Chemical Co. Inv. (Dayton, OH). Zinc nitride (A. R.), silver nitrate (A. R.) and potassium sodium tartrate were purchased from Beijing chemical reagent factory (Beijing, China). All of these chemicals and materials were used as received. Ultrapure water was used throughout the work.

2.2 Formation of DNA networks

λ-DNA networks were prepared with a simple method. Briefly, λ-DNA was diluted to 25 ng μL^{-1} with ultrapure water, and mixed with 10 mM $ZnAc_2 \cdot 2H_2O$ solutions in equal volumes. 20 μL of this DNA solution was dropped onto freshly cleaned indium-tin-oxide (ITO). Ten minutes later, the sample was rinsed with ultrapure water for 30 s and a uniform and nanoporous DNA network formed on the ITO surface.

2.3 Several ZnO NR arrays prepared by seeded growth process

ITO with DNA networks was wetted with a droplet of 0.02 M $ZnAc_2 \cdot 2H_2O$ in ethanol, rinsed with ethanol after 25 s, and blown dry with N_2. This wetting procedure was carried out 0, 2, 4, 6 times, and the sample was heated to 350 °C in air for 20 min in order to yield ZnO seed layers. The ITO slide with ZnO seeds was then vertically immersed into a growth solution (0.025 M $Zn(NO_3)_2$, 0.025 M HMT) and heated to 92.5 °C for 1 h.

2.4 Preparation of SERS-active substrate

The ITO slide with optimized ZnO NR arrays was immersed in an aqueous solution of 0.05 M $AgNO_3$ and was illuminated under monochromatic UV light (365 nm) for 10 min. This immersion and illumination step was repeated and the slide was then illuminated for 30 min. Finally, the substrate was placed into the silver plating solution for 10 min to prepare silver nanoparticles (Ag NPs) on ZnO NR arrays.[31]

2.5 Instruments

SEM images were obtained by field-emission scanning electron microscopy (FESEM, Hitachis-4800). Tapping-mode AFM imaging was performed on a Digital Instruments multimode AFM controlled by Nanoscope IIIa apparatus (Digital Instruments, Santa Barbara, CA) equipped with an E scanner. XRD data were collected on a D/max-RA X-ray spectrometer (Rigaku). UV-vis absorption spectra were collected in solid using a Cary 500 UV-vis-NIR spectrophotometer. Photoluminescence (PL) measurements were performed using a He–Cd laser line of 325 nm as the excitation source. SERS spectra were measured with a Renishaw 2000 model confocal microscopy Raman spectrometer with a CCD detector and a holographic notch filter (Renishaw Ltd., Gloucestershire, U.K.). The microscope attachment was based on a Leica DMLM system, and a 50× objective was used to focus the laser beam onto a spot with approximately 1 μm in diameter. Radiation of 514.5 nm from an air-cooled argon ion laser was used for the SERS excitation. All of the spectra reported were the results of a single 20 s accumulation.

3. Results and discussion

3.1 Controllable synthesis of ZnO seeds on DNA network

Fig. 1a shows an AFM image of a DNA network adsorbed on an ITO surface. Different DNA strands crossed over each other and created compact and uniform reticulated structures. The height of the DNA networks was measured using cross-section analysis, and the histogram of their distribution is shown in Fig. 1b. The statistical histogram shows that the average height of DNA networks was about 1.14 nm, which is 2 times that of a single DNA chain that is reported to be about 0.5 nm by AFM in air.[32,33] The DNA network can be immobilized on ITO because Zn^{2+} acts as a bridge ion between the phosphate groups of DNA and ITO surface. The main immobilization force is the electrostatic attraction between Zn^{2+}, DNA, and ITO. A key factor is that Zn^{2+} should be introduced, which can benefit in two ways. One is that it can make the DNA strands immobilize onto the ITO surface tightly. The other advantage is that the bridge ions (Zn^{2+}) can be decomposited to form ZnO seeds. In our previous work, DNA structures with different concentrations formed on the surface were studied.[34,35] When the DNA concentration is decreased (1–5 ng μL^{-1}), DNA molecules cannot cover the entire surface, and also cannot overlap or cross each other to form a DNA network.[34] When the DNA concentration is increased to more than 20 ng μL^{-1}, more densely packed DNA networks and DNA films can be obtained.[35] Fig. 2a shows ZnO seeds (S1, ESI†) formed by thermally decomposing DNA/Zn^{2+} networks, and the seeds are relatively fat hexangular nanoplatelets with diameter of 50–60 nm. The density of ZnO seeds was estimated to be about 15 per μm^2. In fact, the size of ZnO seeds is much larger than that of the ZnO seeds reported by Yang *et al.*[30] In their previous procedure, zinc acetate dehydrate was adsorbed directly on the substrate, and then was heated to yield layers of ZnO seeds with diameter of 5–20 nm. We suggested that the strong electrostatic interaction between zinc ions and the phosphate backbone of DNA strands could accelerate the nucleation and growth of ZnO nanoparticles. In addition, the as-prepared ZnO seeds are hexangular nanoplatelets, which may favor the further growth of hexagonal end faceted ZnO nanorods.

To examine the effect of the wetting procedure on the growth of ZnO nanorods, the DNA networks were wetted different times with zinc acetate, and then were heated to 350 °C in air for 20 min to yield ZnO seeds. Fig. 2b–d shows the SEM images of ZnO seeds (S2–4) formed on the DNA network when wetting for 2, 4, and 6 times. When the DNA network was wetted 2 times, a little more ZnO nanoparticles were obtained. The density of ZnO seeds was estimated to be about 22 per μm^2. When the wetting times were increased to 4 times, the density of ZnO seeds was increased to about 35 per μm^2. When the wetting times were increased to 6 times, the density of ZnO seeds was as high as about 70 per μm^2. An obvious trend is that the density of ZnO seeds increased as the number of wetting times increased. It is

Downloaded by Changchun Institute of Optics, Fine Mechanics and Physics, CAS on 23 April 2012
Published on 17 May 2011 on http://pubs.rsc.org | doi:10.1039/C1JM10830A

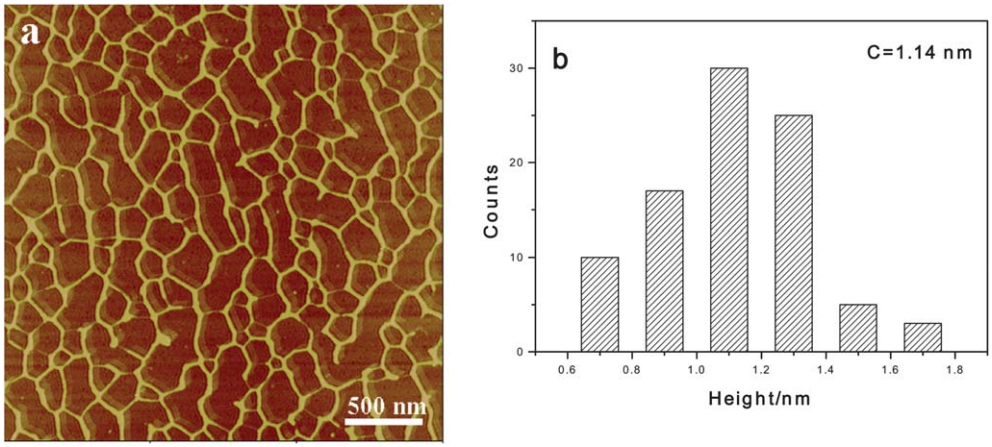

Fig. 1 (a) Tapping mode AFM image of DNA networks, (b) corresponding height distribution histogram of AFM image of (a).

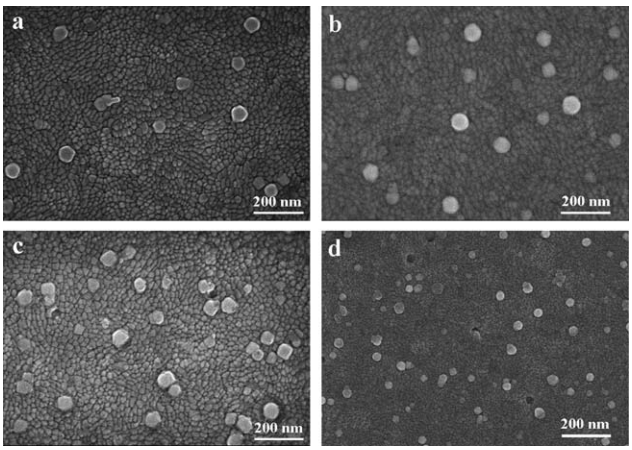

Fig. 2 SEM images of ZnO seeds (S1–4) formed on the DNA network when wetting for (a) 0, (b) 2, (c) 4, and (d) 6 times.

suggested that the number of zinc ions adsorbed on the DNA networks increases with the increasing of the number of wetting times. In our previous work, the effect of Zn^{2+} concentration on DNA morphologies has been studied, and it was found that in the case of low concentration (lower than 10 mM), Zn^{2+} concentration did not greatly change the morphology of DNA networks. After that range, some obvious aggregation between DNA chains appeared.[36] In this work, the DNA network on ITO surface after six times of wetting treatment was imaged by AFM (See Figure S1a†), and a DNA network with obvious aggregation was observed. The height of the DNA networks was about 2.35 nm, which was much larger than DNA networks on ITO before wetting treatment (See Figure S1b†). The increase in height might be possibly due to the formation of DNA bundles with such a high concentration of $ZnAC_2$.

3.2 Formation of ZnO NR arrays using ZnO seeds

Fig. 3 shows SEM images of ZnO NR arrays grown from different ZnO seeds (S1–4) in aqueous solution at 92.5 °C. When ZnO seeds S1 were used, several dispersed ZnO NRs were obtained on the ITO surface (Fig. 3a). The average diameter and length of ZnO NRs were about 150 nm and 600 nm, and the tilt angle was in the range from 20° to 90° with respect to the substrate normal. The density of ZnO NRs was estimated to be about 2 per μm^2. When ZnO seeds S2 were used, clusters with densely packed ZnO NRs were found on the whole ITO surface scanned (Fig. 3b). It was found that the ZnO clusters were composed of more than 30 NRs, in which the roots of the NRs were grown together. The average diameter and length of the ZnO NRs were about 150 nm and 1 μm, and the tilt angle was in the range from 10° to 70° with respect to the substrate normal. Comparing with ZnO NRs grown from S1 seeds, the density was increased to about 10 per μm^2. When ZnO seeds S3 were used, more dense ZnO NR arrays were observed on the ITO surface (Fig. 3c). The average diameter and length of ZnO NRs were about 150 nm and 1 μm, which was similar to that of the ZnO NR arrays shown in Fig. 3b. The tilt angle was in the range from 0° to 60° with respect to the substrate normal, and the ZnO NRs density was increased to about 35 per μm^2. When ZnO seeds S4 were used, highly vertical ZnO NR arrays with diameter of 100–200 nm and length of 1 μm were synthesized (Fig. 3d). The ZnO NRs density was increased to about 48 per μm^2, and the tilt angle was in the range from 0° to 10° with respect to the substrate normal.

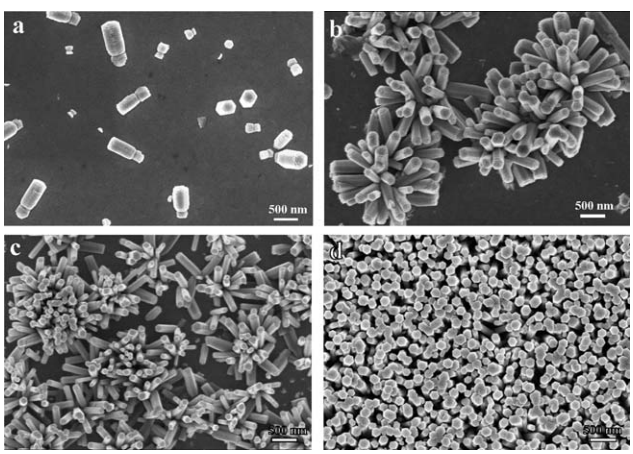

Fig. 3 (a–d) SEM images of ZnO nanorods grown from ZnO seeds (S1–4).

This journal is © The Royal Society of Chemistry 2011

Downloaded by Changchun Institute of Optics, Fine Mechanics and Physics, CAS on 23 April 2012
Published on 17 May 2011 on http://pubs.rsc.org | doi:10.1039/C1JM10830A

It is noticeable that the DNA network pattern has an important influence on the finally resulting ZnO array. When the DNA concentration is very low, as mentioned above, DNA molecules (5 ng μL^{-1}) cannot cover the entire surface, and also cannot overlap or cross each other to form a DNA network (See Figure S2a†). The finally resulting ZnO NRs also cannot cover the entire surface (See Figure S2b†). The average diameter and length of ZnO NRs were about 260 nm and 1.5 μm, respectively, which was similar to that of ZnO NR arrays shown in Fig. 3b. The tilt angle was in the range from 10° to 60° with respect to the substrate normal, and ZnO NRs density was about 10 per μm^2. When the DNA concentration is very high, as mentioned above, DNA molecules (20 ng μL^{-1}) formed more densely packed DNA networks (See Figure S2c†). The finally resulting ZnO NRs were similar with ZnO NR arrays shown in Fig. 3d (Figure S2d†). These results indicate that the ZnO array is sensitive to DNA patterns when the DNA concentration is in the range of 1–5 ng μL^{-1}. When the DNA concentration was above 12.5 ng μL^{-1}, no significant change was observed, indicating that 12.5 ng μL^{-1} DNA is enough to adsorb Zn^{2+} for a vertical ZnO NR array. Therefore, the optimal DNA concentration for ZnO NR array formation should be 12.5 ng μL^{-1}.

In our experiments, ZnO NRs had a strong trend to grow vertically, and the tilt angle of ZnO NRs with respect to the substrate normal depended on the ZnO seeds density, which was controlled by varying the number of wetting times. As the wetting times increased, the ZnO seeds density increased, and the ZnO NRs density increased accordingly. And when the density of ZnO seeds was as high as about 70 per μm^2, completely vertical ZnO NR arrays were obtained over the entire surface of the substrates. It was reported that the vertical NR arrays are highly suitable for use in ordered nanorod-polymer solar cells.[37] In this study, vertical ZnO NR arrays fabricated on the ITO slide have potential applications in photovoltaic devices, and the ITO slide can also act as an electrode. A further study about this is currently underway and will be reported at a later date. We suggested that the quality of ZnO seeds is an important factor for the orientation of ZnO NRs. Similar phenomena have been found by scientists previously. For example, Yang *et al.* found that the orientation of the ZnO seeds directly determines the orientation of the nanorods.[30] To further investigate the effect of ZnO seeds to the formation of ZnO NRs, a 100 nm thick ZnO film fabricated by magnetron sputtering was used as a seed layer. Fig. 4a, b show SEM images of ZnO films formed by magnetron sputtering and ZnO NR arrays grown from these seeds. Fig. 4c shows the high-magnification SEM image of ZnO NRs. The ZnO film consists of nanoparticles with diameter of 20–50 nm, and the density is as high as 400 per μm^2. The ZnO NRs have diameter ranging from 24 to 150 nm and a length of a few micrometres. The NR number density was estimated to be 65 per μm^2 which was much lower than that of seeds. It was suggested that a small part of the seeds contributed to the growth of NRs. Comparing with ZnO NRs from S4 seeds, the NR density was increased, but the tilt angle with respect to the substrate normal was as large as 10–50°. The results further demonstrate that the quality of ZnO seeds is a key factor to determine the orientation of ZnO NRs. In another control experiment, ZnO NRs were grown on an ITO surface with no seeds in aqueous solution at 92.5 °C for 1 h. Fig. 4d shows the SEM image of as-prepared ZnO NRs with

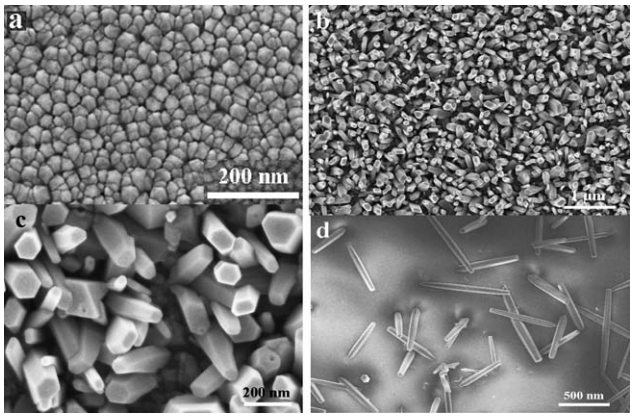

Fig. 4 SEM images of (a) ZnO seeds fabricated by magnetron sputtering, (b) correspondingly grown ZnO nanorods, (d) ZnO nanorods grown with no seeds, (c) high-magnification SEM image of (b).

diameter of 35–65 nm and length of 180–950 nm, separated by gaps of 0–700 nm. The NR number density was as low as 500 per mm^2, which indicates that the existence of ZnO seeds favors the growth of NRs on the substrate.

We have tried different substrates for growing ZnO nanorods, for example, mica, glass, n-type Si (100) and sapphire substrates. It was found that growth of ZnO nanorods is substrate-independent as long as the substrate has a flat surface. Although an ITO slide was used here for ease of imaging, we routinely obtain similar nanorod arrays over the entire surface of all of the substrates mentioned above. See Figure S3 of the Supporting Information† for SEM image and UV-vis absorption spectrum of ZnO NRs on glass grown by the same method. ITO itself is a semiconductor and it is opaque in UV and infrared. The UV-vis absorption and transmission spectra of the pure ITO slide were collected and are shown in Figure S4†. It revealed that the transmission of the ITO slide could reach 70%–84% when the wavelength was larger than 350 nm. As the background of the ITO absorption was removed in testing, thus the absorption of ITO will not affect the results presented in this work.

3.3 Preparation and characterization of ZnO/Ag nanocomposites

In order to prepare SERS-active substrates, we used ZnO NR arrays (shown in Fig. 3d) as templates for preparing ZnO/Ag nanocomposites. Fig. 5a, b show the SEM images of the as-synthesized ZnO/Ag NR arrays. Ag nanoparticles (NPs) were successfully deposited onto the surface of ZnO NRs. The average diameter of Ag NPs is about 18 nm. The successful decoration can be clearly seen in a high-magnification SEM image, as shown in Fig. 5b. Ag NPs were brought together and their interparticle distance was smaller than 5 nm. The number density of Ag NPs on the surface of ZnO NRs was estimated to be about 6 per NR. Ag NPs prefer to attach to the side of the ZnO NRs. Similar phenomena have been found in our previous research.[38] The energy dispersive X-ray spectrum (EDS) (Fig. 5c) confirms that the samples consist of element Zn, O and Ag. The signals of both Zn and O are attributed to the ZnO NRs. The Ag signal results from the Ag nanoparticles on the surface of the ZnO NRs. No

Downloaded by Changchun Institute of Optics, Fine Mechanics and Physics, CAS on 23 April 2012
Published on 17 May 2011 on http://pubs.rsc.org | doi:10.1039/C1JM10830A

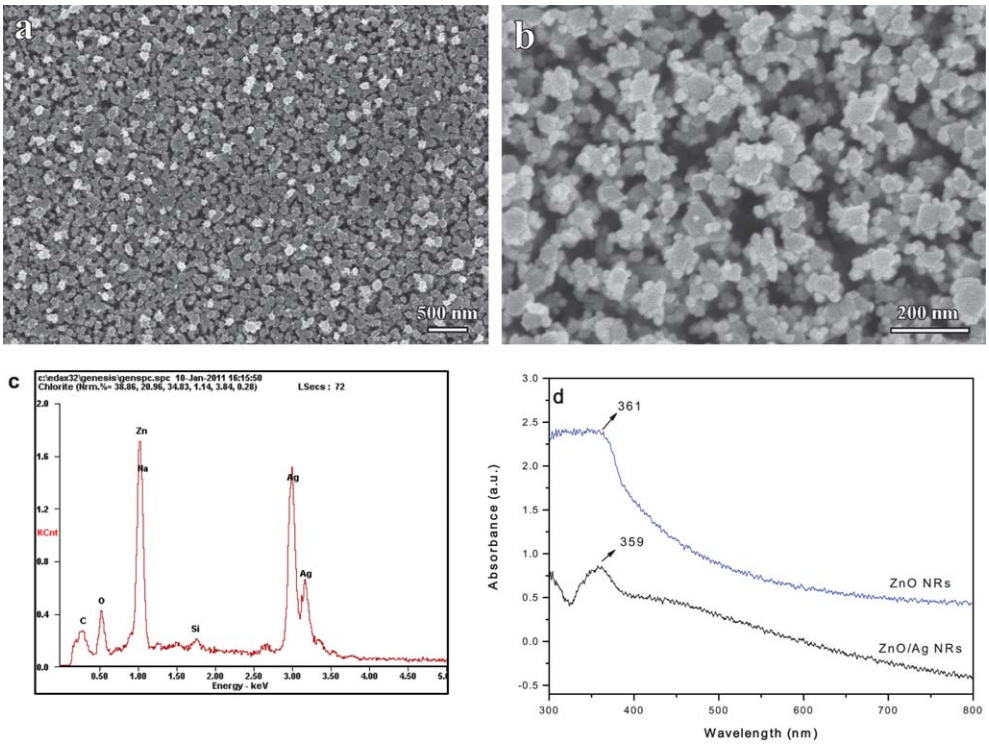

Fig. 5 (a) SEM image and (c) EDS spectrum of ZnO/Ag nanocomposites, (b) High-magnification SEM image of (a), (d) UV-vis absorption spectra of ZnO/Ag nanocomposites and ZnO nanorods.

other signals were observed in the EDS, indicating that the as-prepared sample is pure.

Fig. 5d compares the UV-vis absorption spectra of ZnO/Ag NRs with that of ZnO NRs. For ZnO NRs, the absorption peak between 300 and 400 nm is attributed to the exciton emission of ZnO in the UV light region. In the case of ZnO/Ag NRs, another broad band around 450 nm is observed, indicating the formation of Ag NPs. The peak at 450 nm shows a great red-shift compared with the peak formed by reduction of sodium citrate, which is about 400 nm.[39] It is reasonable that the optical and electronic properties of the metal NPs are dependent on the nanoparticles' size, shape, and environment. It is well known that spherical Ag NPs will display only a single surface plasmon band due to their completely symmetrical shape. But the Ag NPs in ZnO/Ag NRs displayed a wide peak, which may be attributed to the coupling of the plasmon absorbance of the closely spaced Ag NPs. On the other hand, Templeton *et al.* have reported that the position of plasmon absorption is related to electron density of the metal. When the electron density of metal is increased, the plasmon absorption λ of the metal was decreased, leading to the blue-shift of the plasmon absorption band. For a ZnO n-type semiconductor, the work function ($\varphi_{s\ ZnO} \approx 4.3$ eV) is more than that of the noble metals ($\varphi_{m\ Ag} \approx 4.26$). And thus ZnO can donate electrons to Ag readily.[40] Thus, the transfer of electrons from ZnO to Ag occurs until two systems reach a dynamic equilibration, resulting in an increase of electron density of Ag. But in this experiment, the red-shift of the plasmon peak of silver is observed. Therefore, there may be other factors that influence the position of plasmon absorption. For example, the environment of Ag NPs may be a key factor in the position of plasmon absorption. When Ag NPs were adsorbed on the ITO surface, its absorption has a red shift in comparison with that of Ag NPs in colloid. The red-shift of the surface plasmon absorption is attributed to the strong interfacial coupling between Au NPs. A detailed study about the red-shift of the plasmon absorption band will be investigated in future work. In addition, the absorption peak between 300 and 400 nm for ZnO/Ag NRs has a blue-shift compared with that for ZnO NRs. The blue-shift of the surface plasmon absorption (SPR) may be caused by Ag coating on ZnO NRs. Ag NPs act as the molecular linkers between ZnO NRs, and strong interfacial coupling between ZnO NRs caused the blue-shift of the SPR peak.

The purity and crystallinity of the as-synthesized ZnO/Ag NRs were examined by X-ray diffraction (XRD) patterns. Fig. 6 shows the XRD patterns of the ZnO NR arrays and ZnO/Ag NR arrays. From Fig. 6a, it was found that ZnO NRs are crystalline, and the XRD pattern has peaks at $2\theta = 34.6$, 36.4. The 2θ diffraction peaks correspond to (002) and (101) ZnO wurtzite structure facets (JCPDS Card File No. 36-1451). The strong peak at (002) confirmed that the ZnO NRs have a preferred [0001] growth direction.[41] For ZnO/Ag NR arrays, these peaks can still be observed, and a new strong peak at $2\theta = 38.5$ is observed in Fig. 6b. The new peak can be indexed to the (111) plane of the cubic metallic silver (JCPDS Card File No. 04-0783). The above result indicates that Ag NPs have been coated on the surface of ZnO NRs without impurities.

In order to further gain insight to the effect of the Ag NPs in contact with the ZnO NRs, the room temperature PL spectra of ZnO NRs and ZnO/Ag NRs were investigated in Fig. 7. The PL spectrum of ZnO NRs consists of two emission bands in the UV

 This journal is © The Royal Society of Chemistry 2011

Downloaded by Changchun Institute of Optics, Fine Mechanics and Physics, CAS on 23 April 2012
Published on 17 May 2011 on http://pubs.rsc.org | doi:10.1039/C1JM10830A

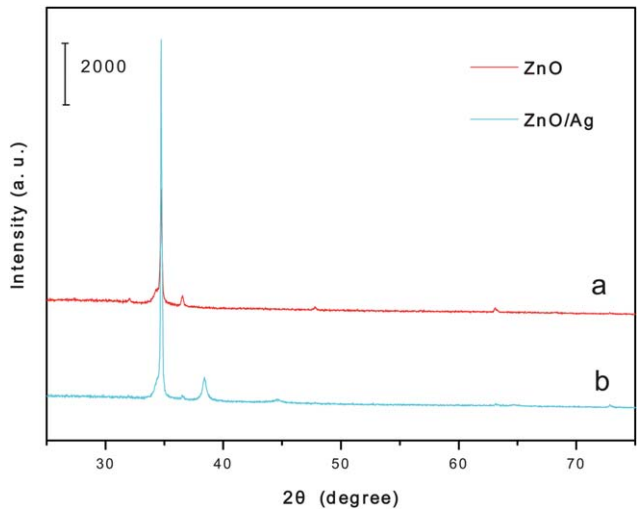

Fig. 6 XRD patterns of (a) ZnO nanorods and (b) ZnO/Ag nanocomposites.

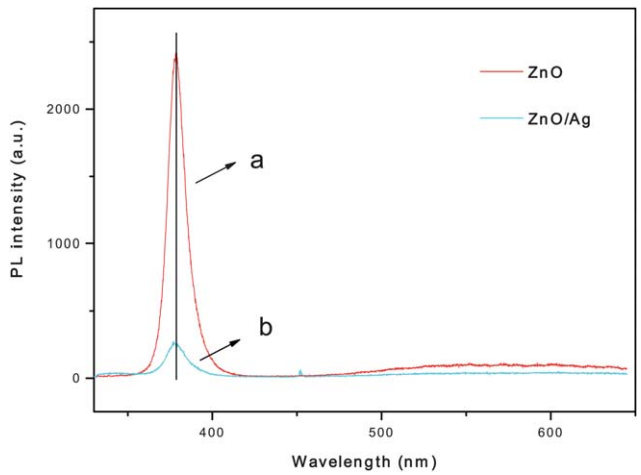

Fig. 7 The RTPL spectra of (a) ZnO nanorods and (b) ZnO/Ag nanocomposites.

and visible regions, respectively. The UV emission band with an asymmetrical lineshape was centered at about 379 nm. The asymmetrical lineshape is attributed to the near-band edge exciton and bound exciton emission. The broad visible emission band around 520 nm is generally related to defect related intrinsic defects like oxygen vacancies, zinc vacancies, oxygen interstitials and zinc interstitials.[42] There are two mechanisms for the visible emission, one is the recombination of a shallowly trapped electron with a deeply trapped hole, and the other one is the recombination of a shallowly trapped hole with a deeply trapped electron.[43] After being decorated with 18 nm Ag NPs, the ZnO NRs display weakened UV and green emission peaks, and the ratio of the UV and green band height decreases from 20 to 8.0. In addition, the PL peak in the UV-region has a slight shift to shorter wavelength, so that is to the high-energy side. It revealed that the growth of Ag NPs onto ZnO NRs almost completely quenches the PL, because the nucleation and growth of Ag nanoparticles may be involved in the defects of the surface, which can trap the photogenerated electrons and holes. Thus we believe that the decrease of the intensity of ZnO visible emission is due to the formation of Ag NPs in oxygen vacancies or defects on the surface of ZnO nanoparticles, which passivates the surface of ZnO. Surface passivation is responsible for an energy potential high enough to prevent surface states trapping the electrons or holes that are photogenerated, which blocks the pathway to form the luminescence centers.

3.4 SERS properties of ZnO/Ag composite nanoarrays

Considering the fact that SERS is often present on aggregated silver nanoparticles in the range of 20–200 nm,[44] the ZnO/Ag NRs are expected to be SERS-active because the Ag NPs aggregates are involved in the nanocomposites. In our experiment, R6G was used as the probe molecule due to its well-established Raman spectral data and the large Raman scattering cross section.[45] It should be noted that the Raman signal of R6G molecules partly contributes to the resonance enhancement (about 2–3 orders of magnitude) of the laser used, such as 514.5 nm argon ion laser used in our work, so the spectrum of R6G detected is actually the surface-enhanced resonance Raman scattering (SERRS) signal. Fig. 8 displays the SERRS spectra for 10^{-10} M R6G adsorbed on the ZnO/Ag NRs, Ag NPs and ZnO NRs complexes at an excitation wavelength of 514.5 nm. For the ZnO/Ag NRs, a low-concentration of R6G produced a clear enhanced effect at 1650 cm^{-1}, one of the main characteristic bands. A detailed assignment of the spectral features of R6G has been reported previously and will not be repeated here.[45] It is noted that the SERS performance of such an ZnO/Ag substrate has been stable for more than 1 month. But the Raman intensity is very weak for pure Ag NPs prepared with the silver-plating method. And no Raman peaks could be observed when the R6G solution was dispersed on the pure ZnO NRs substrate.

The possible reasons for the high Raman intensity enhancement were explained as follows. The SERS enhancement efficiencies depend on the interparticle distance. As stated above, Ag NPs were closed-packed, and their interparticle distance was smaller than 5 nm. When excited by incident light, the collective

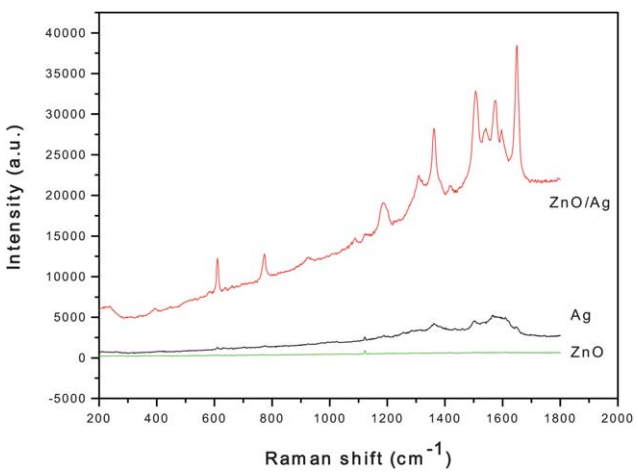

Fig. 8 SERRS spectra of R6G (1×10^{-10} M) on ZnO/Ag nanocomposites, ZnO nanorods and Ag nanoparticles prepared with the silver-plating method. Laser power 25 mW, 1%; integration time: 20 s.

Downloaded by Changchun Institute of Optics, Fine Mechanics and Physics, CAS on 23 April 2012
Published on 17 May 2011 on http://pubs.rsc.org | doi:10.1039/C1JM10830A

surface plasmon is localized at these close-packed silver nanoparticles, resulting in the formation of a local field in this region. The localized resonant plasmon modes can contribute to a larger SERS enhancement. As reported by Sun *et al.*, the SERS effect is mainly due to the interaction between close-packed particles which induces a perturbation of the local electromagnetic (EM) field around each particle.[46] In their work, little enhancement was found for isolated nanoparticles, while a large enhancement was observed for aggregates with multiple particles. This is due to plasmon coupling between nanoparticles in close proximity, which results in huge electromagnetic field enhancements at junction sites or SERS "hot spots". From the above discussions, it is reasonable to conclude that EM field enhancement plays an important role in the SERS enhancement.

3.5 Estimation of the SERS enhancement

To evaluate the SERS activity of the ZnO/Ag composite, 4-ATP was used as the model probe molecule. Fig. 9 shows the normal Raman spectrum of solid 4-ATP and the SERS spectrum of 4-ATP on the ZnO/Ag composite. The normal Raman spectrum of solid 4-ATP is similar to that reported by Osawa *et al.* and Zheng *et al.*[47,48] The γ_{CS} band shifts from 1085 cm^{-1} in Fig. 9a to 1070 cm^{-1} in Fig. 9b, and an obvious Raman frequency shift from 1591 to 1579 cm^{-1} was also observed. These changes of several main bands indicate that the –SH group in 4-ATP makes direct contact with the silver film surface by forming a strong Ag–S bond. The enhancement factor (EF) for 4-ATP on the substrate was calculated according to the equation:

$$EF = (I_{SERS}/I_{Raman})\ (M_{bulk}/M_{surface})$$

where I_{SERS} and I_{Raman} are the intensities in the SERS and normal Raman spectrum, respectively; M_{bulk} is the concentration of molecules in the bulk sample; and $M_{surface}$ is the concentration of adsorbed molecules. For the target molecule 4-ATP, in the sample area (1 μm in diameter) measured, $M_{surface}$ was calculated to be 1.2×10^4 μm^{-2}. Taking the laser spot (1 μm in diameter) and the penetration depth (about 2 μm) and the density of 4-ATP (1.17 g mL^{-1}) into account,[49] M_{bulk} had a value of 0.82×10^{10} μm^{-2} in the detected solid sample area. For the vibrational modes at 1390 cm^{-1} (b_2), EF was estimated to be about 7.4×10^8.

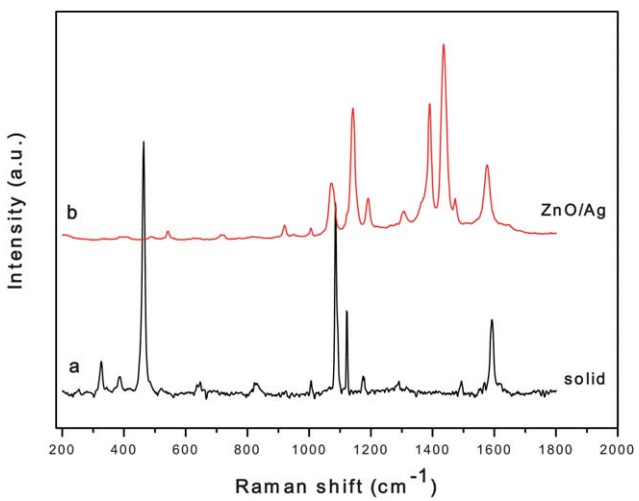

Fig. 9 (a) Normal Raman spectrum of solid 4-ATP, (b) SERS spectrum of 4-ATP (1×10^{-7} M) on ZnO/Ag nanocomposites. Laser power 25 mW, 1%; integration time: 20 s.

The use of our ZnO/Ag NRs composites as a SERS substrate has several advantages. First, the good signal-to-noise for the SERS spectra of R6G and 4-ATP on the ZnO/Ag NRs substrate indicates that the substrate is very suitable as a SERS substrate. In this work, we thought the Raman enhancement is mainly ascribed from SERS "hot spots" between two close-packed Ag NPs and the relatively large surface area provided by the ZnO NR arrays. Second, the ZnO/Ag nanocomposites have good stability and reproducibility.

4. Conclusions

We have developed a controllable seeded synthetic method for fabrication of ZnO NR arrays in mild conditions using DNA networks as templates. In the synthesis, the final density of ZnO NRs is determined mainly by that of the ZnO seed. By forming ZnO seeds on a DNA network, highly vertical NR arrays free of intermediate thin films or nanoparticles layers were fabricated. The DNA network plays an important role not only as a substrate for the adsorbing of zinc ions, but also as a fine template for density controllable synthesis of high-quality ZnO seeds. The density of ZnO seeds became larger when the wetting times were increased. By introduction of Ag NPs on the surface of ZnO NRs, ZnO/Ag nanocomposites can be prepared easily, which provides an opportunity to fabricate stable and reproducible SERS-active substrates. The enhancement factor for ZnO/Ag nanocomposites is as high as about 7.4×10^8 with 4-ATP as the probe molecule.

Acknowledgements

This work was supported by the Key Project of National Natural Science Foundation of China under Grant No. 50532050, the China Postdoctoral Science Foundation No. 20100481068.

References

1 E. Braun, Y. Eichen, U. Sivan and G. Ben-Yoseph, *Nature*, 1998, **391**, 775.
2 T. Torimoto, M. Yamashita, S. Kuwabata, T. Sakata, H. Mori and H. Yoneyama, *J. Phys. Chem. B*, 1999, **103**, 8799.
3 W. E. Ford, O. Harnack, A. Yasuda and J. M. Wessels, *Adv. Mater.*, 2001, **13**, 1793.
4 J. Richter, R. Seidel, R. Kirsch, M. Mertig, W. Pompe, J. Plaschke and H. K. Schackert, *Adv. Mater.*, 2000, **12**, 507.
5 C. F. Monson and A. T. Woolley, *Nano Lett.*, 2003, **3**, 359.
6 G. Lu, P. Maragakis and E. Kaxiras, *Nano Lett.*, 2005, **5**, 897.
7 P. Atanasova1, T. Weitz, P. Gerstel, V. Srot, P. Kopold, P. A. van Aken, M. Burghard and J. Bill, *Nanotechnology*, 2009, **20**, 365302.
8 L. Dong, T. Hollis, B. A. Connolly, N. G. Wright, B. R. Horrocks and A. Houlton, *Adv. Mater.*, 2007, **19**, 1748.
9 L. Levina, V. Sukhovatkin, S. Musikhin, S. Cauchi, R. Nisman, D. P. Bazett-Jones and E. H. Sargent, *Adv. Mater.*, 2005, **17**, 1854.
10 V. Stsiapura, A. Sukhanova, A. Baranov, M. Artemyev, O. Kulakovich, V. Oleinikov, M. Pluot, J. H. M. Cohen and I. Nabiev, *Nanotechnology*, 2006, **17**, 581.
11 A. G. Wu, Z. Li, H. L. Zhou, J. P. Zheng and E. K. Wang, *Analyst*, 2002, **127**, 585.
12 G. Wei, H. L. Zhou, Z. G. Liu, Y. H. Song, L. L. Sun, T. Yang and Z. Li, *J. Phys. Chem. B*, 2005, **109**, 23941.

 This journal is © The Royal Society of Chemistry 2011

View Online

13 M. H. Huang, S. Mao, H. Feick, H. Yan, Y. Wu, H. Kind, E. Weber, R. Russo and P. Yang, *Science*, 2001, **292**, 1897.
14 E. M. C. Fortunato, P. M. C. Barquinha, A. C. M. B. G. Pimentel, A. M. F. Goncalves, A. J. S. Marques, L. M. N. Pereira and R. F. P. Martins, *Adv. Mater.*, 2005, **17**, 590.
15 T. Mitsuyu, S. Ono and K. J. Wasa, *Appl. Phys.*, 1980, **51**, 2646.
16 J. M. Baik and J. L. Lee, *Adv. Mater.*, 2005, **17**, 2745.
17 Z. L. Wang, *Adv. Mater.*, 2003, **15**, 432.
18 U. Ozgur, Y. I. Alivov, C. Liu, A. Teke, M. A. Reshchikov, S. Dogan, V. Avrutin, S.-J. Cho and H. J. Morkoc, *J. Appl. Phys.*, 2005, **98**, 041301.
19 Y. K. Tseng, C. J. Huang, H. M. Cheng, I. N. Lin, K. S. Liu and I. C. Chen, *Adv. Funct. Mater.*, 2003, **13**, 811.
20 Q. H. Li, Y. J. Chen, Q. Wan and T. H. Wang, *Appl. Phys. Lett.*, 2004, **85**, 1805–1807.
21 B. Pall and M. Sharan, *Mater. Chem. Phys.*, 2002, **76**, 82.
22 L. M. Chen, L. B. Luo, Z. H. Chen, M. L. Zhang, J. A. Zapien, C. S. Lee and S. T. Lee, *J. Phys. Chem. C*, 2010, **114**, 93.
23 N. Audebrand, J. P. Auffredic and D. Louer, *Chem. Mater.*, 1998, **10**, 2450.
24 Y. R. Lin, S. S. Yang, S. Y. Tsai, H. C. Hsu, S. T. Wu and I. C. Chen, *Cryst. Growth Des.*, 2006, **6**, 1951.
25 B. Cheng and E. T. Samulski, *Chem. Commun.*, 2004, 986.
26 H. L. Cao, X. F. Qian, Q. Gong, W. M. Du, X. D. Ma and Z. K. Zhou, *Nanotechnology*, 2006, **17**, 3632.
27 M. H. Huang, Y. Y. Wu, H. Feick, N. Tran, E. Weber and P. D. Yang, *Adv. Mater.*, 2001, **13**, 113.
28 Z. Q. Tian, J. A. Voigt, J. Liu, B. Mckenzie and M. J. Mcdermott, *J. Am. Chem. Soc.*, 2002, **124**, 12954.
29 O. Taratula, E. Galoppini and R. Mendelsohn, *Langmuir*, 2009, **25**, 2107.
30 L. E. Greene, M. Law, D. H. Tan, M. Montano, J. Goldberger, G. Somorjai and P. D. Yang, *Nano Lett.*, 2005, **5**, 1231.
31 B. Zhang, H. Wang, L. Lu, K. Ai, G. Zhang and X. Cheng, *Adv. Funct. Mater.*, 2008, **18**, 2348.
32 T. Thundat, D. P. Allison and R. J. Warmack, *Nucleic Acids Res.*, 1994, **22**, 4224.
33 H. Z. Zheng, D. W. Pang, Z. X. Lu, Z. L. Zhang and Z. X. Xie, *Biophys. Chem.*, 2004, **112**, 27.
34 G. Wei, L. Wang, H. L. Zhou, Z. G. Liu, Y. H. Song and Z. Li, *Appl. Surf. Sci.*, 2005, **252**, 1189.
35 Y. H. Song, Z. Li, Z. G. Liu, G. Wei, L. Wang, L. L. Sun, C. L. Guo, Y. J. Sun and T. Yang, *J. Phys. Chem. B*, 2006, **110**, 10792.
36 Y. H. Song, C. L. Guo, L. L. Sun, G. Wei, C. Y. Peng, L. Wang, Y. J. Sun and Z. Li, *J. Phys. Chem. B*, 2007, **111**, 461.
37 B. D. Yuhas and P. D. Yang, *J. Am. Chem. Soc.*, 2009, **131**, 3756.
38 L. L. Sun, D. X. Zhao, M. Ding, Z. K. Xu, Z. Z. Zhang, B. H. Li and D. Z. Shen, preparation.
39 V. Subramanian, E. E. Wolf and P. V. Kamat, *J. Phys. Chem. B*, 2003, **107**, 7479.
40 C. H. Ye, Y. S. Bando, X. S. Fang, G. Z. Shen and D. Golberg, *J Phys. Chem. C*, 2007, **111**, 12673.
41 B. Liu and H. C. Zeng, *Nano Res.*, 2009, **2**, 201.
42 Y. G. Wang, S. P. Lau, H. W. Lee, S. F. Yu and B. K. Tay, *J. Appl. Phys.*, 2003, **94**, 1.
43 A. V. Dijken, E. A. Meulenkamp, D. Vanmaekelbergh and A. Meijerink, *J. Lumin.*, 2000, **90**, 123.
44 D. J. Maxwell, S. R. Emory and S. Nie, *Chem. Mater.*, 2001, **13**, 1082.
45 K. Kneipp, H. Kneipp, I. Itzkan, R. R. Dasari and M. S. Feld, *Chem. Rev.*, 1999, **99**, 2957.
46 T. Xiao, Q. Ye and L. Sun, *J. Phys. Chem. B*, 1997, **101**, 632.
47 M. Osawa, N. Matsuda, K. Yoshll and I. Uchida, *J. Phys. Chem.*, 1994, **98**, 12702.
48 J. Zheng, X. Li, R. Gu and T. Lu, *J. Phys. Chem. B*, 2002, **106**, 1019.
49 H. Z. Yu, J. Zhang, H. L. Zhang and Z. F. Liu, *Langmuir*, 1999, **15**, 16.

Downloaded by Changchun Institute of Optics, Fine Mechanics and Physics, CAS on 23 April 2012
Published on 17 May 2011 on http://pubs.rsc.org | doi:10.1039/C1JM10830A